

# Quantitative intravital microscopy using a Generalized Polarity concept for kidney studies

Weiming Yu, Ruben M. Sandoval, and Bruce A. Molitoris

Nephrology Division, Department of Medicine, Indiana University School of Medicine, Indianapolis, Indiana

Submitted 26 April 2005; accepted in final form 8 June 2005

**Yu, Weiming, Ruben M. Sandoval, and Bruce A. Molitoris.** Quantitative intravital microscopy using a Generalized Polarity concept for kidney studies. *Am J Physiol Cell Physiol* 289: C1197–C1208, 2005. First published July 20, 2005; doi:10.1152/ajpcell.00197.2005.—In this article, we describe a ratiometric intravital two-photon microscopy technique for studying glomerular permeability and differences in proximal tubule cell reabsorption. This quantitative approach is based on the Generalized Polarity (GP) concept, in which the intensity difference between two fluorescent molecules is normalized to the total intensity produced by the two dyes. After an initial intravenous injection of a mixture of 3-, 40-, and 70-kDa fluorescently labeled dextrans into live Munich-Wistar-Frömter (MWF) rats, we were able to monitor changes in the GP values between any two dyes within local regions of the kidney, including the glomerulus, Bowman's capsule, proximal tubule lumens and proximal tubule cells, and individual capillary vessels. We were able to quantify accumulations of different dextrans in the Bowman's space and in tubular lumens as well as reabsorption by proximal tubular cells at different time points in the same rat. We found that for 6- to 8-wk-old MWF rats that developed spontaneous albuminuria, the 40- and 70-kDa dextrans, with hydrodynamic radii larger than albumin, were differentially filtered, but both were able to pass the glomerular filtration barrier and enter into the urinary space of the Bowman's capsule within a few seconds after intravenous infusion. Using GP image analysis, we found that negatively charged dextrans of both 40 and 70 kDa were better reabsorbed by the proximal tubule cells than the neutrally charged 40-kDa dextran. These results demonstrate the potential power of the GP imaging technique for quantitative studies of glomerular filtration and tubular reabsorption.

glomerular permeability; tubular reabsorption; charge selectivity; two-photon excitation; multiphoton

SINCE THE INCEPTION of two-photon fluorescence microscopy in the early 1990s (9), significant progress has been made in applying this imaging technique in *in vivo* studies. Recently, the possibility of using two-photon excitation fluorescence microscopy to scan the kidney in live animals and viable tissues has been demonstrated (10, 22, 23). There is great potential application for this imaging technique in the study of kidney diseases such as ischemic acute renal failure (16, 30, 31) and for studying molecular trafficking and drug metabolism inside the kidney (26, 32). Normal functions of the kidney are directly associated with filtration, reabsorption, and excretion for the regulation of salt and water content of the body, removing waste products, and maintaining normal blood chemistry. Two-photon fluorescence microscopy holds particular promise for the study of these functions because it allows observation of local regions of the kidney, such as the glomerulus, the proximal tubule cells, and distal tubule cells with

subcellular and submicron resolution together with nanomolar concentration sensitivity (11).

Intravital microscopy is becoming increasingly important in studying kidney functions and associated disease processes. However, our interpretation and understanding of the data are hindered by a lack of quantitative imaging techniques. It was previously suggested that by infusing a bulk solution of selected fluorescent dyes into the animal, one could use two-photon fluorescence microscopy over time to evaluate drug and dye molecules' filtration process, transit and transport processes of these molecules in the renal tubules (10), and microvascular permeability within the kidney (30). Quantitative evaluation of these processes is essential. However, it is typically difficult to use fluorescence intensity directly for quantification because of intensity fluctuations caused by local and temporal changes in kidney hemodynamics and processing of the fluorescent molecules. In this report, we describe a ratiometric imaging technique based on a Generalized Polarity (GP) concept that compares the relative intensities of two fluorescent dyes and the use of GP imaging to quantify relative molecular distribution of fluorescently labeled dextrans within local regions of the kidney at selective time intervals after dye infusion. This GP imaging technique with two-photon excitation was originally developed for the quantitative study of local lipid packing and dynamics of biological membranes (35). Similarly to other ratiometric imaging techniques, GP imaging is sensitive to relative concentration changes of the two fluorescent probes and is advantageous for studying processes involving extensive and rapid concentration changes such as those related to glomerular filtration and tubular reabsorption. It is relatively insensitive to the amount of fluorescent probe injected and the depth of field imaged. In this report, we demonstrate the use of this imaging technique for studying permeability across the glomerulus and the reabsorptive property of tubular epithelial cells *in vivo*.

## MATERIALS AND METHODS

The GP function has the same form as the polarization function (35). Assume that we used a mixture of two fluorescent molecules, *A* and *B*, for infusion and that the molecular weight of *A* is larger than that of *B*. On those bases, we defined the GP function as follows:

$$GP_{A/B} = \frac{I_{A(\text{large})} - I_{B(\text{small})}}{I_{A(\text{large})} + I_{B(\text{small})}} \quad (1)$$

where  $I_{A(\text{large})}$  and  $I_{B(\text{small})}$  are the fluorescence intensities emitted from molecules *A* and *B*, respectively. By definition, the GP value has a minimum value of  $-1$  and a maximum value of  $+1$ . If, within a

Address for reprint requests and other correspondence: W. Yu, Nephrology Division, Dept. of Medicine, Indiana Univ. School of Medicine, 950 W. Walnut St., R2-268, Indianapolis, IN 46202 (e-mail: wmyu@iupui.edu).

The costs of publication of this article were defrayed in part by the payment of page charges. The article must therefore be hereby marked "advertisement" in accordance with 18 U.S.C. Section 1734 solely to indicate this fact.

local region, there is a dominant amount of the larger molecule (GP approximately +1) or the smaller molecule (GP approximately -1), we considered this region to be highly polarized, meaning that there was a large separation between the molecular distribution of the larger molecule, *A*, and that of the smaller molecule, *B*. Similarly, if the GP value of an area is  $\sim 0$ , we considered that there was a minimum separation of the molecular distribution between the two molecules within this area; in other words, low polarity. In practice, we considered an area to have low polarity if its GP value was distributed around the GP value of the dye mixture before infusion, defined as  $GP_0$ . With this definition, the pixel value of GP is an indication of the degree of relative occupation between the two molecules within a given pixel.

**Animal preparation.** Experimental procedures in which we used animals were approved by the Institutional Animal Care and Use Committee and were performed in accordance with the National Institutes of Health's *Guide for the Care and Use of Laboratory Animals*. Male Munich-Wistar-Frömter (MWF) rats (6–8 wk old,  $\sim 200$  g body wt; Harlan, Indianapolis, IN) were used. First, animals were anesthetized by administering an intraperitoneal injection of thiobutabarbital (130 mg/kg; Sigma, St. Louis, MO), shaved, and placed onto a homeothermic table to maintain the animals' body temperature at 37°C. After ensuring adequate anesthesia had been administered, a femoral venous catheter was placed for injection of fluorescent dye solutions. One of the kidneys was exteriorized for microscopic imaging via a 10- to 15-mm lateral incision made dorsally under sterile conditions as previously described (10). In cases in which male Sprague-Dawley rats (6–8 wk; Harlan) are specifically mentioned in the experiments, they were prepared and imaged using the same procedures described above.

**Fluorescent probes.** FITC-conjugated dextrans (40- and 70-kDa mol wt, anionic), tetramethylrhodamine-conjugated dextran (40-kDa mol wt, neutral), cascade blue-conjugated dextran (3,000 mol wt, anionic), and Hoechst 33342 were purchased from Invitrogen-Molecular Probes (Eugene, OR) and dissolved in 0.9% saline. The isoelectric points (IP) of the FITC- and cascade blue-conjugated dextrans were 4.58 and 3.81, respectively.

**Fluorescence microscopy.** A 0.5-ml mixture of fluorescent saline solution containing a total of 1.6 mg/ml FITC-conjugated dextran, 1.6 mg/ml tetramethylrhodamine-conjugated dextran, and 1.6 mg/ml cascade blue-conjugated dextran was infused through the femoral venous catheter immediately before microscopic imaging. In some animals, Hoechst 33342 was used to highlight cellular nuclei and infused as a 400- $\mu$ l saline solution containing 0.6 mg of the dye 10 min before imaging. Microvascular images of the kidney were captured using a two-photon laser-scanning fluorescence microscope system (MRC-1024MP; Bio-Rad Laboratories, Hercules, CA) equipped with a Nikon Diaphot inverted microscope (Fryer, Huntley, IL) according to the procedures described earlier (10). Baseline kidney images were collected before dextran infusion to record autofluorescence signals within the tissue under investigation. All intravital kidney images were acquired using a  $\times 60$  magnification/1.2 numerical aperture water-immersion objective and three external non-scan detectors. The Ti-sapphire laser was adjusted to 800 nm for excitation. The fluorescent dye mixtures prepared for infusion were diluted and imaged using the same illumination and detection settings used for live kidney

imaging. The body temperature of the animals was maintained at 37°C during all imaging procedures.

**Image data analysis.** GP images were calculated using Meta Imaging Series (version 6; Universal Imaging, West Chester, PA) on a personal computer. A threshold level for each detection channel was set according to the average pixel value of an area without significant autofluorescence from images taken before dye infusion. For molecular distribution analysis, an image obtained to show the pixel values ( $\Delta GP$ ) was calculated as follows at each pixel *i*:

$$\Delta GP_{(A/B)i} = \frac{I_{A(\text{large}),i} - I_{B(\text{small}),i}}{I_{A(\text{large}),i} + I_{B(\text{small}),i}} - GP_{(A/B)0,i} \quad (2)$$

where  $GP_{(A/B)0}$  is the corresponding GP image of the fluorescent dextran mixture for each animal infusion. This operation defines the relative shift between the center of the  $GP_{(A/B)}$  distribution of local regions with respect to that of  $GP_{(A/B)}$  of the dextran mixture injected [ $GP_{(A/B)0}$ ].  $\Delta GP_{(A/B)} = 0$  when the dye concentration ratio of a region was the same as the amount being injected.  $\Delta GP_{(A/B)}$  was shifted to either a negative or a positive value, depending on the *A*-to-*B* concentration ratio changes with respect to that of the injected dextran mixture. A valid GP value at a given pixel was calculated only when the corresponding pixel values in both channels for recording signals from *A* and *B* were above their respective threshold levels. The  $\Delta GP$  of a whole image or region of interest (ROI) were exported into PSI-PLOT (version 6; Salt Lake City, UT) for histogram analysis. Image processing was performed in an equivalent manner for all images to ensure that the results were directly comparable.

## RESULTS

### *Distributions of dextran molecules in the proximal tubules.*

First, we investigated the possibility of differential reabsorption of filtered dextrans by proximal tubule cells. As shown in Fig. 1, fluorescent dextrans were reabsorbed by the epithelia of different proximal tubules at different ratios. For example, the color of *area 1* shown in Fig. 1A is reddish and different from the color of *area 2*. This can be observed also in the  $\Delta GP$  images. In Fig. 1B, *area 1*, shown in light blue, had lower average  $\Delta GP_{70 \text{ kDa}/40 \text{ kDa}}$  value (listed in Table 1) than that of *area 2*, which is shown mostly in green. The  $\Delta GP_{70 \text{ kDa}/40 \text{ kDa}}$  distribution of *area 1* (Fig. 1B') was shifted toward smaller values and approached the 100% accumulation level of the smaller molecule (in this case, the 40-kDa dextran) indicated by the blue dotted and dashed line, with  $\Delta GP = -0.84$ . For *area 2*, the  $\Delta GP_{70 \text{ kDa}/40 \text{ kDa}}$  distribution was shifted away from the blue dotted and dashed line that indicated a relatively lower amount of the 40-kDa molecule present in this area. This suggests that proximal tubule 1 reabsorbed more of the fraction of the 40-kDa dextran and less of the 70-kDa dextran than did proximal tubule 2. For  $\Delta GP_{70 \text{ kDa}/3 \text{ kDa}}$ , there were still differences among different proximal tubules (comparing the  $\Delta GP$  distributions of *areas 1* and *2* in Fig. 1C' and their average  $\Delta GP$  values in Table 1). *Area 1* still had smaller average

Fig. 1. Intensity,  $\Delta GP$  images, and local  $\Delta GP$  distributions of kidney microvasculature of a live Munich-Wistar-Frömter (MWF) rat at 36 min after dextran infusion. *A*: three-color combined images (red, 40-kDa dextran; green, 70-kDa dextran; and blue, 3-kDa dextran). Regions of interest (ROI) of 5 selected areas are indicated. *Area 1*, proximal tubule (ROI as indicated); *area 2*, proximal tubule (ROI similar to *area 1*); *area 3*, distal tubule (whole area is ROI); *area 4*, distal tubule (whole area is ROI); and *area 5*, blood vessel lumen (whole area is ROI). *B*:  $\Delta GP_{70 \text{ kDa}/40 \text{ kDa}}$  image. *B'* and *B''*:  $\Delta GP_{70 \text{ kDa}/40 \text{ kDa}}$  distributions of ROI for *areas 1–5* in *A*. The blue and red dotted and dashed lines represent the average  $\Delta GP_{70 \text{ kDa}/40 \text{ kDa}}$  values of the 40- and 70-kDa dextrans alone, respectively. *C*:  $\Delta GP_{70 \text{ kDa}/3 \text{ kDa}}$  image. *C'*:  $\Delta GP_{70 \text{ kDa}/3 \text{ kDa}}$  distributions of ROI (*area 1*, green solid; *area 2*, red solid; *area 3*, purple dash; *area 4*, blue dash). The blue and red dotted and dashed lines represent the average  $\Delta GP_{70 \text{ kDa}/3 \text{ kDa}}$  values of the 3- and 70-kDa dextrans alone, respectively. *D*:  $\Delta GP_{40 \text{ kDa}/3 \text{ kDa}}$  image. *D'*:  $\Delta GP_{40 \text{ kDa}/3 \text{ kDa}}$  distributions of ROI (*area 1*, green solid; *area 2*, red solid; *area 3*, purple dash; *area 4*, blue dash). The blue and red dotted and dashed lines represent the average  $\Delta GP_{40 \text{ kDa}/3 \text{ kDa}}$  values of the 3- and 40-kDa dextrans alone, respectively. All  $\Delta GP$  values are displayed in pseudocolor with a range as indicated. Scale bar in *A*, 20  $\mu$ m.

$\Delta GP_{70 \text{ kDa}/3 \text{ kDa}}$  than that of *area 2*, suggesting that less of the fraction of the 70-kDa dextran was reabsorbed in *area 1*. The fact that the  $\Delta GP_{70 \text{ kDa}/3 \text{ kDa}}$  distributions of the proximal tubules were approaching the average  $\Delta GP_{70 \text{ kDa}/3 \text{ kDa}}$  value of

the 3-kDa molecule alone (shown as a blue dashed line at  $\Delta GP$  approximately  $-1$  in Fig. 1C'), suggests that the 3-kDa molecule was preferentially reabsorbed by the proximal tubules between the 70- and 3-kDa dextran molecules. This was likely

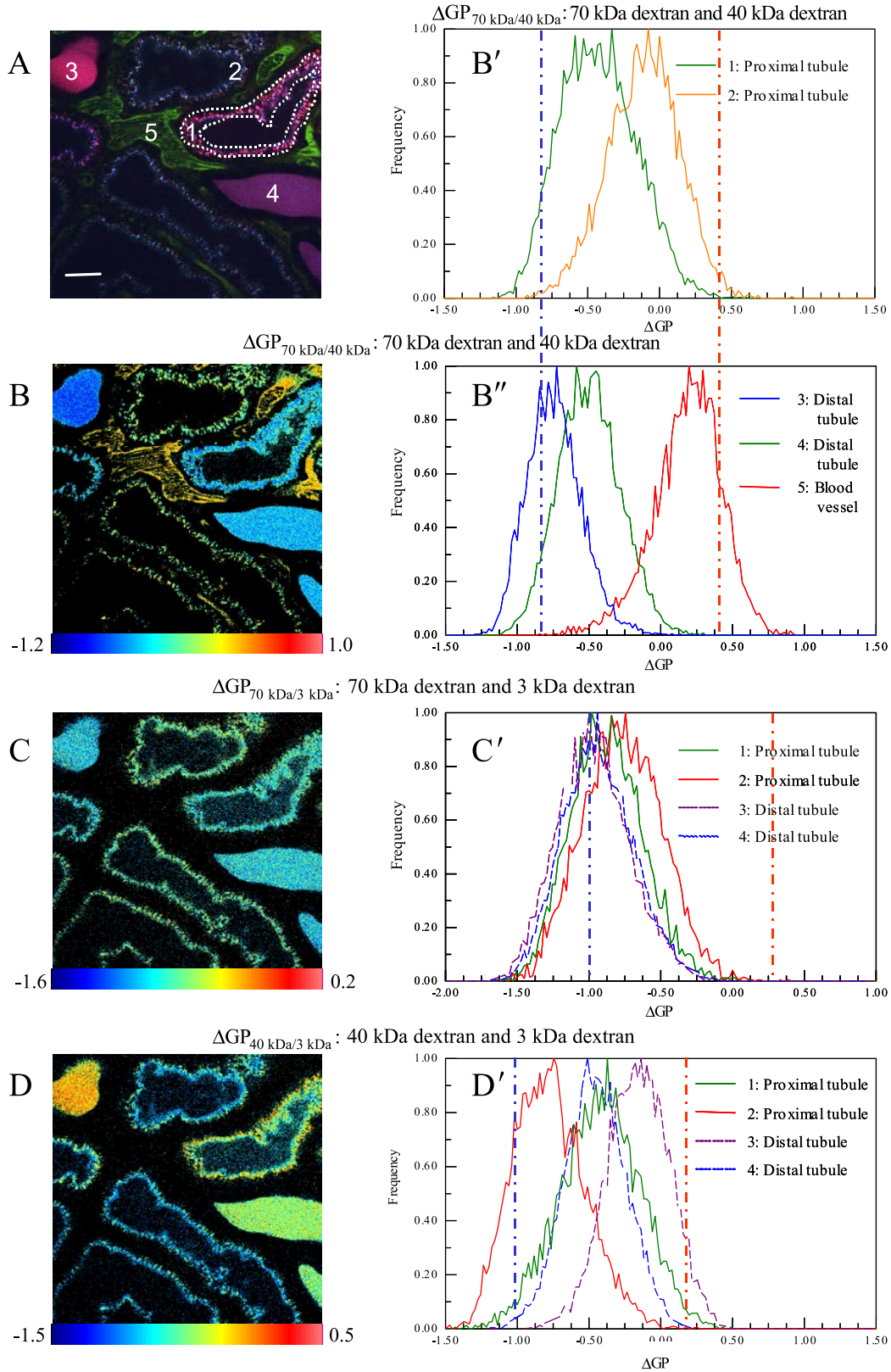


Table 1. 36 min after dextran infusion

$\Delta$ GP	Proximal Tubules		Distal Tubules		Blood Vessels, Area	100%, 70 kDa	100%, 40 kDa	100%, 3 kDa
	Area 1	Area 2	Area 3	Area 4	5			
$\Delta$ GP <sub>70 kDa/40 kDa</sub> , ± FWHM	-0.42±0.263	-0.11±0.25	-0.735±0.19	-0.495±0.215	0.186±0.24	0.413±0.16	-0.84±0.141	
$\Delta$ GP <sub>70 kDa/3 kDa</sub> , ± FWHM	-0.869±0.252	-0.763±0.274	-0.96±0.253	-0.929±0.248		0.289±0.167		-0.98±0.245
$\Delta$ GP <sub>40 kDa/3 kDa</sub> , ± FWHM	-0.421±0.285	-0.769±0.252	-0.155±0.218	-0.451±0.213			0.183±0.158	-1.04±0.202

Data are from regions of interest (ROI) in Fig. 1.  $\Delta$ GP, change in generalized polarity; FWHM, full width at half-maximum.

caused by the presence of overwhelming amounts of the 3-kDa dextran in tubular lumens. The differences between relative accumulations of the 40- and 3-kDa dextrans by the different proximal tubules as well as within a proximal tubule are shown in Fig. 1D. For proximal tubule 1 (*area 1* in Fig. 1A), we observed scattered areas with relatively high  $\Delta$ GP values (shown in reddish color in Fig. 1D) that appeared to be more frequent at locations away from the tubular lumen. To the contrary, the areas with relatively lower  $\Delta$ GP values (shown in greenish color) were closer to the lumen. This suggests that the 40- and 3-kDa dextrans were not reabsorbed and/or processed equivalently by the proximal tubular epithelial cells. *Area 2* (Fig. 1D) shows a pattern similar to that of *area 1* in that there was a relatively higher accumulation of the 3-kDa molecules at the locations near the lumen than at areas away from the lumen and toward the basolateral side of the proximal epithelium. The overall molecular distribution of the proximal tubular epithelium from *area 2* also approached the average  $\Delta$ GP<sub>40 kDa/3 kDa</sub> value of the 3-kDa dextran alone (blue dashed line at  $\Delta$ GP approximately  $-1$  in Fig. 1D'). These results indicate that highly heterogeneous individual proximal tubules reabsorb different dextrans at different ratios at a given time. This heterogeneity depends on the reabsorptive properties of different proximal tubular cells and is likely time and segment dependent after concentration changes of the dextrans in the lumens.

**Molecular distributions in the distal tubules and in the capillary vessels.** We observed different relative molecular distributions between the 70- and 40-kDa dextrans among different distal tubules. This observation is shown in Fig. 1B in the different colors in *areas 3* and *4* of the pseudocolor-coded image. The relatively high levels of molecular accumulations of the 40-kDa dextran are shown in Fig. 1B', where the  $\Delta$ GP<sub>70 kDa/40 kDa</sub> distributions of both tubules were approaching the average  $\Delta$ GP value of the 100% level of accumulation for the 40-kDa dextran. In contrast to the distal tubules, the  $\Delta$ GP<sub>70 kDa/40 kDa</sub> distribution of the blood vessel shown in Fig. 1B'' (*area 5* indicated in Fig. 1A) was shifted toward high values, indicating a higher level of the 70-kDa dextran accumulation than that of the 40-kDa dextran. When comparing the 70-kDa dextran with the 3-kDa dextran, it is clear that the presence of the 3-kDa molecule in the distal tubules was overwhelming. The fact that the  $\Delta$ GP distributions of *areas 3* and *4* in Fig. 1C' closely overlapped indicates that the molecular ratios between the 70- and 3-kDa dextrans were about the same in both tubule lumens at this time point.

**Evaluation of glomerular permeability.** At 4 s after infusion, the three fluorescent dextrans had already entered the urinary

space of the Bowman's capsule, an area indicated by the white arrows shown in all three images (Fig. 2, A1–A3). The  $\Delta$ GP image in Fig. 2C confirms that both the 70- and 40-kDa dextrans were present in Bowman's space. It can also be observed that both of these dextran molecules were already in the lumens of the proximal tubules (indicated by white arrows in Fig. 2C) at this time. This finding indicates that the glomeruli of MWF rats were relatively leaky for both the 70- and 40-kDa dextrans. This may not be surprising for the following two reasons. First, MWF rats have spontaneous albuminuria (28, 29), and second, the asymmetrical molecular shape and the deformability of dextran lead to large dextran molecules crossing the glomerular permeability barrier (33).

The  $\Delta$ GP<sub>70 kDa/40 kDa</sub> distributions (Fig. 2C') of the Bowman's space (*area 1*) and of the proximal tubular lumen (*area 2*) were similar. This suggests, as expected, that the molecular ratios of the two dextrans within the two locations were close at this time point. The difference between the two  $\Delta$ GP<sub>70 kDa/40 kDa</sub> distributions was that the one for the proximal tubular lumen (with an average  $\Delta$ GP<sub>70 kDa/40 kDa</sub> =  $-0.193$ ; see Table 2) was shifted toward smaller  $\Delta$ GP values (compared with an average  $\Delta$ GP<sub>70 kDa/40 kDa</sub> =  $-0.177$  for Bowman's space). Both average  $\Delta$ GP values were obtained by averaging  $>5,000$  pixels, and this difference was significant. These data suggest enhanced loss of the 70-kDa anionic dextran molecule compared with the 40-kDa neutral dextran when it traveled from Bowman's space to the proximal tubule.

Within the blood vessel, the  $\Delta$ GP<sub>70 kDa/40 kDa</sub> distribution was around zero (with an average  $\Delta$ GP<sub>70 kDa/40 kDa</sub> =  $0.092$ ). This indicates that the molecular ratio between the 70- and 40-kDa dextrans was close to that of the dextran mixture used for infusion at this time point. Clearly, the  $\Delta$ GP<sub>70 kDa/40 kDa</sub> distribution of the Bowman's space was shifted toward a lower value compared with that of the blood plasma (Fig. 2C'). This suggests that the 40-kDa dextran passed through the glomeruli relatively faster than the 70-kDa dextran.

The molecular ratio between the 70- and 3-kDa dextrans in Bowman's space was close to that of the proximal tubule as shown in Fig. 2, D and D'. However, by comparing the  $\Delta$ GP<sub>70 kDa/3 kDa</sub> distributions of *area 1* (average  $\Delta$ GP<sub>70 kDa/3 kDa</sub> =  $-0.659$ ) and *area 2* (average  $\Delta$ GP<sub>70 kDa/3 kDa</sub> =  $-0.723$ ) in Fig. 2D', the  $\Delta$ GP distribution from the proximal tubular lumen was shifted toward smaller values. This suggests an increased accumulation of the 3-kDa molecule relative to the amount of the 70-kDa dextran in the proximal tubular lumen. These data further suggest that at 4 s after dye infusion, the 70-kDa dextran was already being reabsorbed by the proxi-

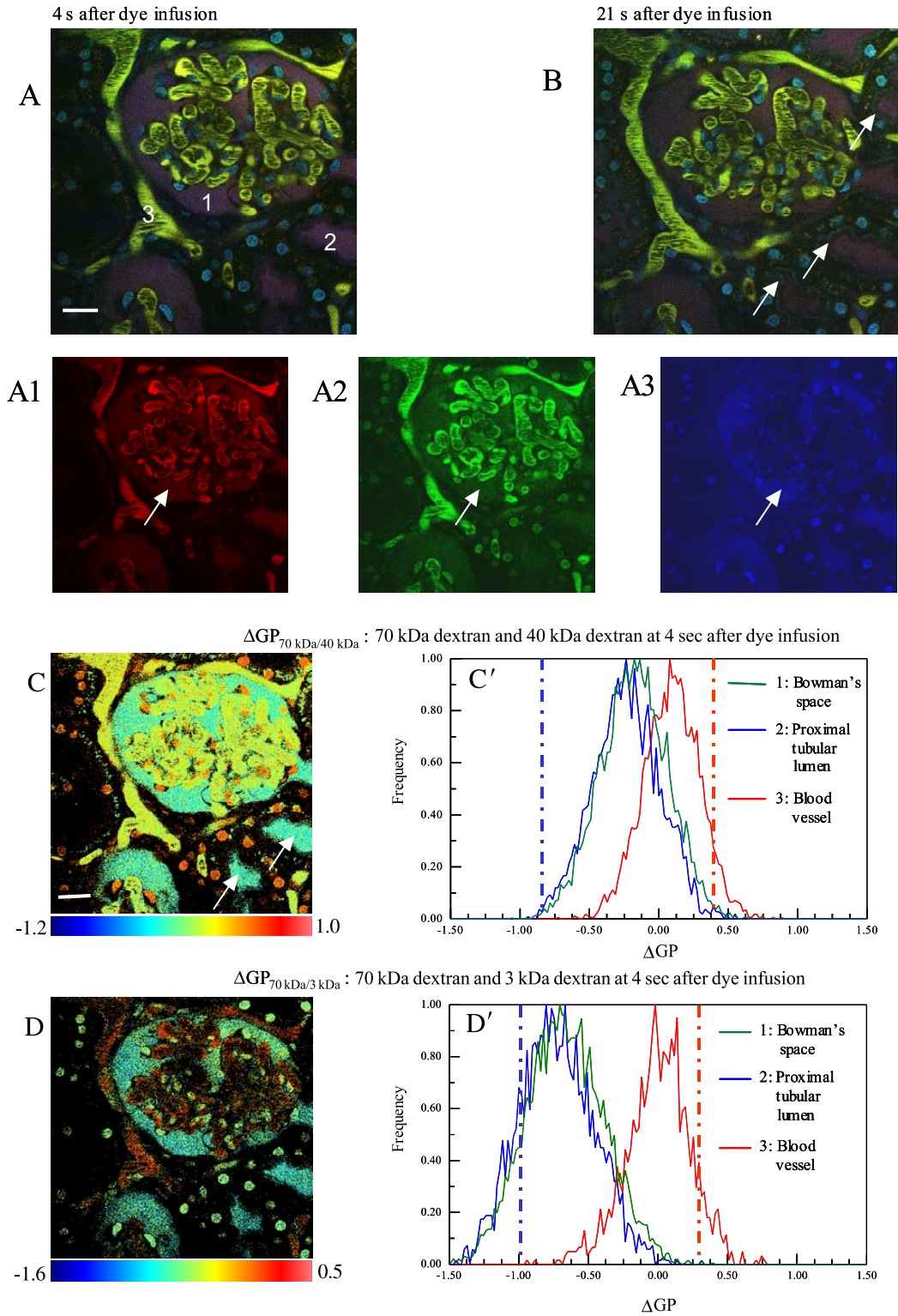


Fig. 2. Intensity,  $\Delta GP$  images, and local  $\Delta GP$  distributions of a glomerulus and surrounding vascular structures of a MWF rat kidney. *A*: three-color combined image at 4 s after dextran infusion (red, 40-kDa dextran; green, 70-kDa dextran; and blue, 3-kDa dextran). ROI analyses were performed on indicated areas. *Area 1*, Bowman's space; *area 2*, proximal tubular lumen; and *area 3*, blood vessel lumen. *B*: three-color combined image at 21 s after dextran infusion. *A1–A3*, intensity images of the 40-kDa tetramethylrhodamine dextran, 70-kDa FITC-dextran, and 3-kDa cascade blue dextran, respectively, at 4 s after dextran infusion. *C*:  $\Delta GP_{70\text{ kDa}/40\text{ kDa}}$  image. *C'*:  $\Delta GP_{70\text{ kDa}/40\text{ kDa}}$  distributions of three selected areas. *Area 1*, green; *area 2*, blue; and *area 3*, red. The blue and red dotted and dashed lines represent the average  $\Delta GP_{70\text{ kDa}/40\text{ kDa}}$  values of the 40- and 70-kDa dextrans alone, respectively. The scattered red areas are nuclei of endothelial cells labeled with Hoechst 33342. *D*:  $\Delta GP_{70\text{ kDa}/3\text{ kDa}}$  image. *D'*:  $\Delta GP_{70\text{ kDa}/3\text{ kDa}}$  distributions of the 3 selected areas. *Area 1*, green; *area 2*, blue; and *area 3*, red. The blue and red dotted and dashed lines represent the average  $\Delta GP_{70\text{ kDa}/3\text{ kDa}}$  values of the 3- and 70-kDa dextrans alone, respectively. All  $\Delta GP$  values are displayed in pseudocolor with the range indicated. Scale bars in *A* and *C*, 20  $\mu\text{m}$ .

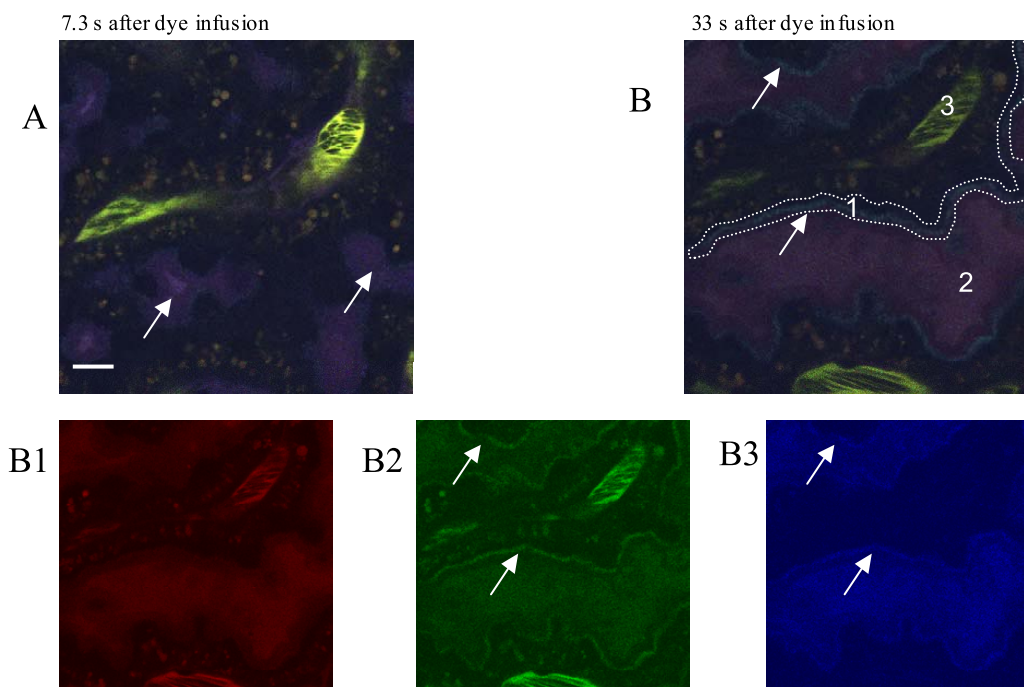


Fig. 3. Intensity,  $\Delta GP$  images, and local  $\Delta GP$  distributions of a proximal tubule and surrounding vascular structures. *A*: three-color combined image at 7.3 s after dextran infusion (red, 40-kDa dextran; green, 70-kDa dextran; and blue, 3-kDa dextran). *B*: three-color combined image at 33 s after dextran infusion. ROI analyses were performed on indicated areas. *Area 1*, proximal brush border; *area 2*, proximal tubular lumen; and *area 3*, blood vessel lumen. *B1–B3*, intensity images of the 40-kDa tetramethylrhodamine dextran, 70-kDa FITC dextran, and 3-kDa cascade blue dextran, respectively, at 33 s after dextran infusion. *C*:  $\Delta GP_{70 \text{ kDa}/40 \text{ kDa}}$  image. *C'*:  $\Delta GP_{70 \text{ kDa}/40 \text{ kDa}}$  distributions of three selected areas. *Area 1*, green; *area 2*, blue; and *area 3*, red. The blue and red dotted and dashed lines represent the average  $\Delta GP_{70 \text{ kDa}/40 \text{ kDa}}$  values of the 40- and 70-kDa dextrans alone, respectively. *D*:  $\Delta GP_{70 \text{ kDa}/3 \text{ kDa}}$  image. *D'*:  $\Delta GP_{70 \text{ kDa}/3 \text{ kDa}}$  distributions of two selected areas. *Area 1*, green; and *area 2*, blue. The blue and red dotted and dashed lines represent the average  $\Delta GP_{70 \text{ kDa}/3 \text{ kDa}}$  values of the 3- and 70-kDa dextrans alone, respectively. *E*:  $\Delta GP_{40 \text{ kDa}/3 \text{ kDa}}$  image. *E'*:  $\Delta GP_{40 \text{ kDa}/3 \text{ kDa}}$  distributions of the 2 selected areas. *Area 1*, brush-border membrane, blue; and *area 2*, proximal tubular lumen, green. The blue and red dotted and dashed lines represent the average  $\Delta GP_{40 \text{ kDa}/3 \text{ kDa}}$  values of the 3- and 40-kDa dextrans alone, respectively. All  $\Delta GP$  values are displayed in pseudocolor with the range indicated. Scale bars in *A* and *C*, 10  $\mu\text{m}$ .

mal tubular epithelial cells. The separation between the  $\Delta GP_{70 \text{ kDa}/3 \text{ kDa}}$  distributions from the blood vessel and that from Bowman's space in Fig. 2*D'* was relatively large (compared with those in Fig. 2*C'*). This is consistent with the fact that a smaller molecule, such as the 3-kDa dextran molecule, passes through the glomeruli relatively faster than a 40-kDa molecule (average  $\Delta GP_{40 \text{ kDa}/3 \text{ kDa}} = -0.502$  in the Bowman's space).

**Molecular reabsorption by the proximal tubular brush-border membrane.** Binding of the dextran molecules by the brush-border membrane of the proximal tubular epithelium was already visible (areas indicated by white arrows in Fig. 2*B*) at 21 s after dextran infusion.

To better visualize and understand the molecular distributions within proximal tubular cells, we acquired local images using a  $\times 2$  zoom with a  $\times 60$  magnification objective (Fig. 3).

Table 2. 4 s after dextran infusion

$\Delta GP$	Area 1, Bowman's Space	Area 2, Proximal Tubular Lumen	Area 3, Blood Vessel
$\Delta GP_{70 \text{ kDa}/40 \text{ kDa}}$ , $\pm$ FWHM	$-0.177 \pm 0.241$	$-0.193 \pm 0.24$	$0.092 \pm 0.203$
$\Delta GP_{70 \text{ kDa}/3 \text{ kDa}}$ , $\pm$ FWHM	$-0.659 \pm 0.28$	$-0.723 \pm 0.270$	$0.04 \pm 0.234$
$\Delta GP_{40 \text{ kDa}/3 \text{ kDa}}$ , $\pm$ FWHM	$-0.502 \pm 0.242$	$-0.513 \pm 0.229$	$-0.081 \pm 0.2294$

Data are from ROI indicated in Fig. 2.

We observed the presence of the fluorescent molecules in the proximal tubular lumen (areas indicated by white arrows in Fig. 3*A*) a few seconds after fluorescent dextran infusion. Thirty-three seconds after dextran infusion, the accumulation of the fluorescent molecules by the proximal tubular epithelial cells was visible (areas indicated by white arrows in Fig. 3*B*). We observed significant accumulations of the negatively charged 70- and 3-kDa dextrans by the apical membrane (areas indicated by white arrows in Fig. 3, *B2* and *B3*). The 40-kDa dextran (neutrally charged) was not reabsorbed well by the apical membrane, because its fluorescence intensity in the apical membrane was lower than that from the lumen (Fig. 3*B1*).

Relatively large accumulations of the 70-kDa dextran, compared with those of the 40-kDa dextrans, were observed as demonstrated in Fig. 3*C*. The molecular distribution within the brush-border membrane was largely shifted toward high  $\Delta GP_{70 \text{ kDa}/40 \text{ kDa}}$  values, with an average  $\Delta GP = 0.195$  (Table 3). This suggests a significantly higher accumulation of the 70-kDa dextran than that of the 40-kDa dextran. This result is consistent with the fact that there were more 40-kDa molecules in the proximal tubular lumen, an area shown with a relatively lower  $\Delta GP_{70 \text{ kDa}/40 \text{ kDa}}$  value (average  $\Delta GP_{70 \text{ kDa}/40 \text{ kDa}} = -0.089$ ; Fig. 3*C* and *histogram 2* in Fig. 3*C'*). Shift of the  $\Delta GP_{70 \text{ kDa}/40 \text{ kDa}}$  distribution from within the blood vessel (*curve 3* in Fig. 3*C'*) toward large values indicates loss of the 40-kDa dextran from the bloodstream because of glomerular filtration. This finding is also consistent with the fact that there

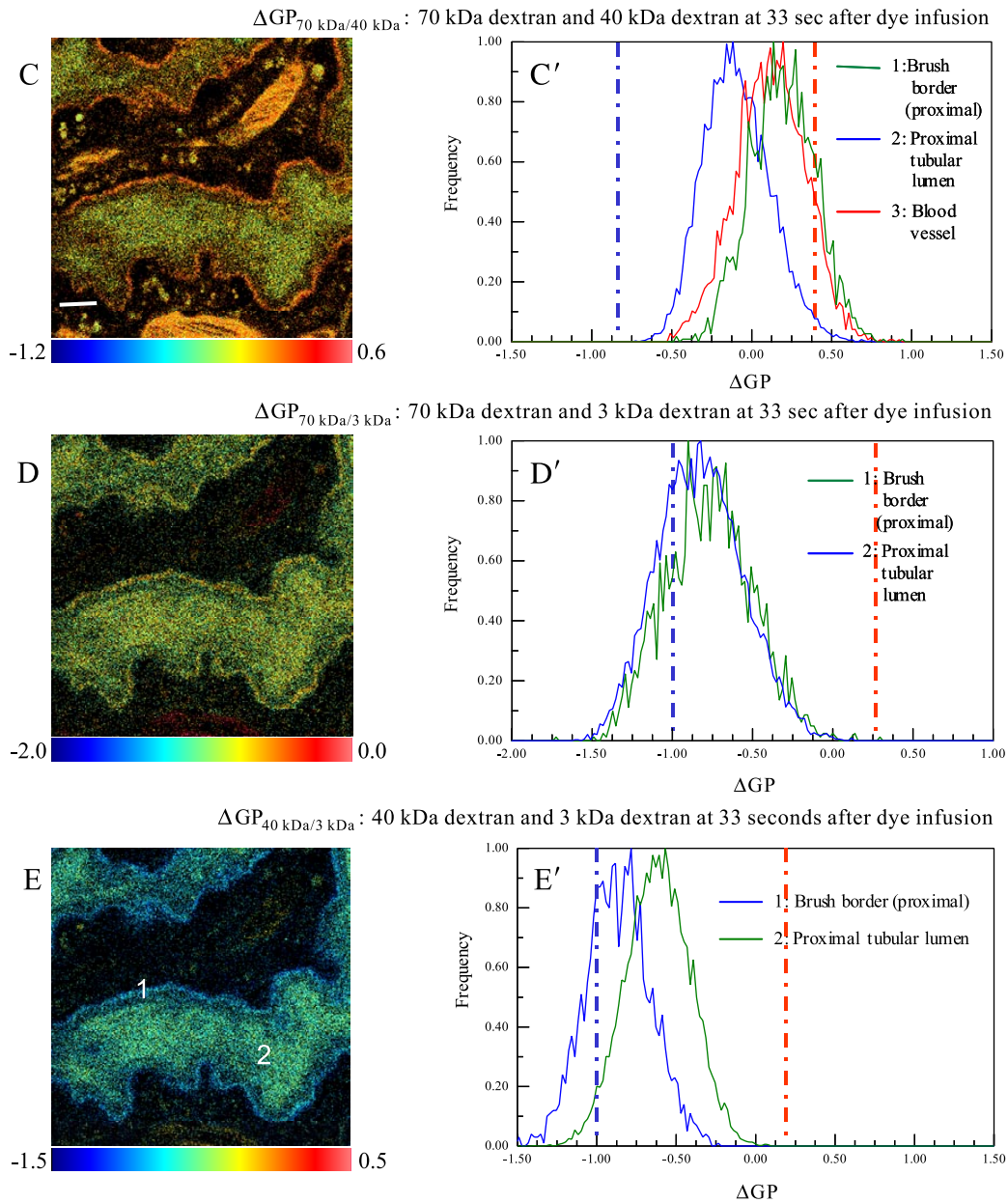


Fig. 3. Continued.

was a significant amount of the 40-kDa molecules in the proximal tubular lumen.

The relative molecular distributions of the 70- and 3-kDa dextrans within *area 1* (apical membrane) and *area 2* (proxi-

mal tubular lumen) were similar (Fig. 3, *D* and *D'*). This suggests that the reabsorption rates of the two molecules by the proximal tubular cells were similar and were independent of the size of the molecules being reabsorbed. The  $\Delta GP$  distributions of both the lumen and the brush-border membrane of the proximal tubule, shown in Fig. 3, *D* and *D'*, were shifted toward low values. This indicates that although at this time point there were significant amounts of the 70-kDa dextran present in the lumen and being reabsorbed by the epithelial cells, the presence of the 3-kDa dextran in the proximal tubules and therefore the filtration of this relatively small molecule by the kidney was dominant.

Relative molecular distributions of the 40- and 3-kDa dextrans in the proximal tubular lumen was different from those in the apical membrane (Fig. 3, *E* and *E'*). The  $\Delta GP_{40 \text{ kDa}/3 \text{ kDa}}$  distribution from the proximal tubular lumen was shifted to-

Table 3. 33 s after dextran infusion

$\Delta GP$	Area 1, Brush-Border Membrane	Area 2, Proximal Tubular Lumen	Area 3, Blood Vessel
$\Delta GP_{70 \text{ kDa}/40 \text{ kDa}}$ , $\pm$ FWHM	$0.195 \pm 0.202$	$-0.089 \pm 0.207$	$0.122 \pm 0.217$
$\Delta GP_{70 \text{ kDa}/3 \text{ kDa}}$ , $\pm$ FWHM	$-0.766 \pm 0.272$	$-0.822 \pm 0.265$	
$\Delta GP_{40 \text{ kDa}/3 \text{ kDa}}$ , $\pm$ FWHM	$-0.860 \pm 0.204$	$-0.611 \pm 0.203$	

Data are from ROI indicated in Fig. 3.

ward larger values than those from the apical membrane. These data suggest that the 40-kDa-to-3-kDa molecular ratio was higher in the lumen than that in the brush-border membrane. This finding again indicates that the proximal tubule cells did not reabsorb the 40-kDa neutral dextran well compared with the 3-kDa anionic dextran.

$\Delta GP$  from within the blood vessel and the interstitium. The  $\Delta GP_{70 \text{ kDa}/40 \text{ kDa}}$  distributions (Fig. 4, A and B) from within a blood vessel and the interstitial space next to it were within the 100% accumulation lines for the 70-kDa dextran (red dashed line) and for the 40-kDa dextran (blue dashed line). This

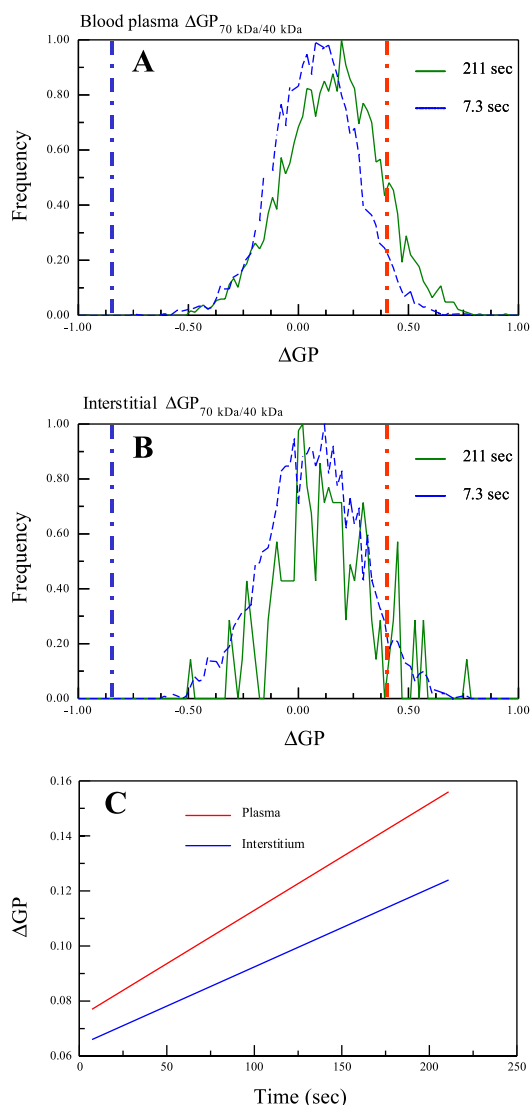


Fig. 4.  $\Delta GP$  of blood plasma and from interstitial space. A:  $\Delta GP_{70 \text{ kDa}/40 \text{ kDa}}$  distributions of blood plasma at 7.3 s (blue dashed line) and at 211 s (green solid line) after dextran infusion. B:  $\Delta GP_{70 \text{ kDa}/40 \text{ kDa}}$  distributions from interstitial space at 7.3 s (blue dashed line) and at 211 s (green solid line) after dextran infusion. C: plot showing  $\Delta GP_{70 \text{ kDa}/40 \text{ kDa}}$  as functions of time using the average  $\Delta GP_{70 \text{ kDa}/40 \text{ kDa}}$  values listed in Table 4. ROI ( $\sim 7,000$ – $10,000$  pixels) represents the blood plasma that was selected from the blood vessel shown in Fig. 3A. The blue and red dotted and dashed lines represent the average  $\Delta GP_{70 \text{ kDa}/3 \text{ kDa}}$  values of the 40- and 70-kDa dextrans alone, respectively. The ROI of the interstitial space was selected directly around the blood vessel, and we were able to select an area of only  $\sim 900$  pixels from the 211-s  $\Delta GP$  image.

Table 4. Average change in GP values

Time Course	Interstitium		Blood Plasma	
	$\Delta GP_{70 \text{ kDa}/40 \text{ kDa}}$	FWHM	$\Delta GP_{70 \text{ kDa}/40 \text{ kDa}}$	FWHM
7.3 s	0.066	0.218	0.077	0.189
211 s	0.124	0.204	0.156	0.216

Data are from ROI indicated in Fig. 4.

suggests that both of these molecules were present within the blood vessel and the interstitial space. The increase in the average  $\Delta GP$  values at 211 s with respect to those at 7.3 s for both the blood plasma and the interstitium (Fig. 4D) indicates an increase in the 70-kDa-to-40-kDa molecular ratio within this time window. This finding was expected because the 40-kDa dextran was cleared faster than the 70-kDa dextran from the plasma. The slope plotted in Fig. 4C for the plasma using the average  $\Delta GP$  values shown in Table 4 (see also Fig. 4) was relatively larger than the slope for the interstitial space. This suggests that the rate of increasing the 70-kDa-to-40-kDa molecular ratio as a function of time was relatively faster from within the blood vessel than that from the interstitial space. It is likely that the 40-kDa dextran was removed more slowly from the interstitium than from the plasma, although both the 70- and 40-kDa dextrans were able to enter into the interstitial space. This indicates that the 40- and 70-kDa dextrans were not freely exchanged between the blood vessel and the interstitial space.

## DISCUSSION

*GP value and channel cross talk.* Similarly to other ratio-metric imaging techniques, the GP value is affected by the intensity levels of both channels A and B ( $I_A$  and  $I_B$  from Eq. 1). Therefore, the GP value depends on the instrument settings and the degree of channel cross talk as well as on the relative concentrations of the dye that contribute to the signals in channels A and B. Considering channel cross talk, GP has the following form:

$$GP = \frac{(I_A + f_{BA}I_B) - (I_B + f_{AB}I_A)}{(I_A + f_{BA}I_B) + (I_B + f_{AB}I_A)} \quad (3)$$

where  $f_{BA}I_B$  is the intensity from molecule B (due to cross talk) that contributes to the total intensity of channel A, and  $f_{AB}I_A$  is the intensity from molecule A that contributes to the total intensity of channel B.  $f_{BA}$  and  $f_{AB}$  are fractions (typically, they are  $< 1$ ). Figure 5 is a plot of GP as a function of the intensity ratio  $I_A/I_B$ . As shown in Fig. 5, GP reaches a plateau when  $I_A \gg I_B$ . The GP value of the plateau depends on the level of channel cross talk; in this particular example, it is  $f_{AB}I_A$ . When  $f_{AB}$  increases, the GP value of the plateau decreases (Fig. 5, dashed line). The GP value reaches the minimum when  $I_A \ll I_B$ . The GP value of this minimum also depends on the cross-talk signal  $f_{BA}I_B$ . When  $f_{BA}$  increases, the minimum GP value increases (Fig. 5, dotted and dashed line). The GP range is thus reduced as a result of channel cross talk. Among the three fluorescent probes we used, the major cross talk was produced by FITC-conjugated dextran and its fluorescence appeared in all three imaging channels. There was almost no cross talk to the cascade blue channel from the other two dextrans. This was the reason why the average  $\Delta GP$  lines of the

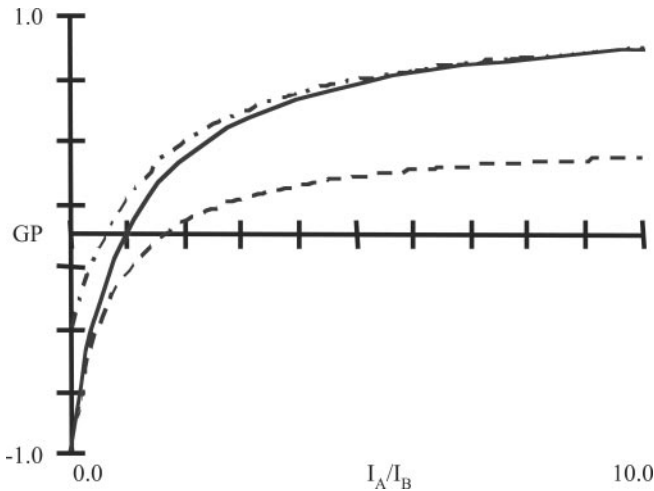


Fig. 5. Effect of channel cross talk on the dynamic range of GP from theoretical calculations using Eq. 4. Solid line, no cross talk,  $f_{AB} = 0$  and  $f_{BA} = 0$ . Dashed line,  $f_{AB} = 0.38$  and  $f_{BA} = 0$ . Fluorescence signal from molecule A in channel B is 38% of the fluorescence signal of molecule A detected in channel A. Dotted and dashed line,  $f_{AB} = 0$  and  $f_{BA} = 0.38$ . Fluorescence signal from molecule B in channel A is 38% of the fluorescence signal of B detected in channel B.

3-kDa cascade blue-conjugated dextran alone on the  $\Delta GP$  plots were about  $-1$  in Figs. 1–3. The fact that the average  $\Delta GP$  lines in Figs. 1–3 for either the 70-kDa FITC dextran or 40-kDa rhodamine dextran alone were not at  $-1$  or  $+1$  was due to fluorescence contributions from other dextrans.

Considering the effects of instrument settings and other experimental conditions, GP has the following general form:

$$GP = \frac{G_I(G_D I_{0A} + f_{BA} I_{0B}) - (G_{Df_{AB}} I_{0A} + I_{0B})}{G_I(G_D I_{0A} + f_{BA} I_{0B}) + (G_{Df_{AB}} I_{0A} + I_{0B})} \quad (4)$$

where  $G_I$  is the instrument factor and  $G_D$  is a dye factor that accounts for variables that affect dye intensity, such as chromophore concentration, quantum yield, and so forth.  $I_{0A}$  and  $I_{0B}$  are normalized intensity values from a single chromophore. The differences of the instrument factor among different instrument settings can be obtained by measuring the GPs from samples containing single fluorescent dye molecules. Both G factors can be determined experimentally when needed to

compare GP values obtained from different experimental conditions. In practice, we compared the GP value differences with respect to the GP of the dye mixture using the same instrument settings (Eq. 2).

Autofluorescence can contribute to alteration of the calculated GP values. There was relatively strong autofluorescence from the epithelium of the proximal tubules when imaged using two-photon excitation at  $\sim 800$  nm. It is difficult to remove the autofluorescence from a GP image of a kidney after dye infusion unless the exact locations of the autofluorescence are known. In Fig. 6, we plotted a GP distribution of the autofluorescence measured before dye infusion (using signals obtained from detection channels for the 70-kDa FITC dextran and 40-kDa tetramethylrhodamine dextran), together with the  $\Delta GP_{70 \text{ kDa}/40 \text{ kDa}}$  distribution from the proximal tubular epithelium. Because the GP distribution of the autofluorescence was around zero, the effect of autofluorescence on the measured  $\Delta GP$  was to move the average  $\Delta GP$  value toward 0 and to contribute to the  $\Delta GP$  distributions  $\sim 0$ . There were no significant autofluorescence signals from other regions of the kidney.

*Glomerular leakage of dextrans with large molecular weight.* The MWF rat we used is a genetic model that develops spontaneous albuminuria (28). Its urinary albumin excretion increases significantly during the maturation of the animal between 8 and 14 wk of age (28, 29). This rat is an excellent model for studying kidney functions associated with progressive glomerular injury and abnormal glomerular filtration (14, 15, 18). Despite the extensive efforts made to characterize the functional and structural alterations in this animal model, the genetic and structural origins that directly lead to the development of spontaneous albuminuria in the animal are still unclear. It was evident from our GP imaging experiments that the 3- and 40-kDa dextrans, as well as the 70-kDa dextran, were present in both Bowman’s space and the proximal tubules shortly after infusion. The fluorescence signals from the Bowman’s space, as well as from the proximal tubule lumen, were strong and cannot be accounted for as signals from unbound fluorescent tag molecules. By infusing a mixture of fluorescent dextrans previously dialyzed for 24 h to remove free fluorescent tag molecules, we obtained the same results as reported herein. The  $\Delta GP$  values listed in Table 2 indicate that in the Bowman’s space at 4 s after dextran infusion,  $\Delta GP_{70 \text{ kDa}/3 \text{ kDa}}$

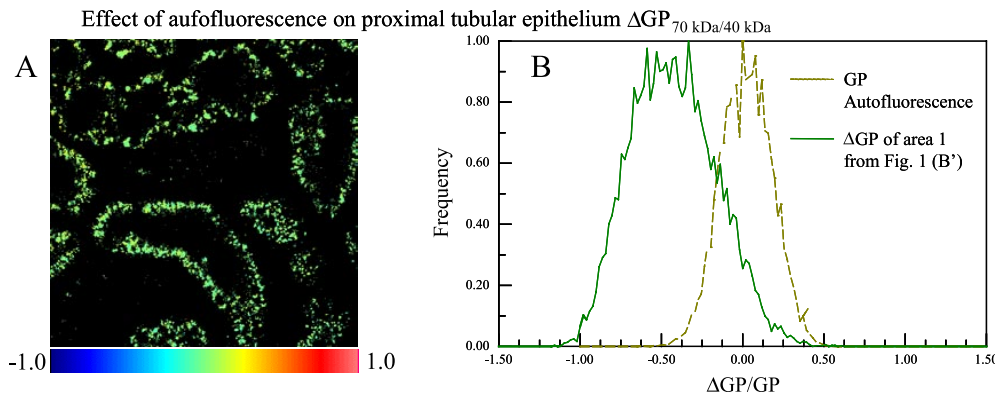


Fig. 6. Comparison of autofluorescence GP and  $\Delta GP_{70 \text{ kDa}/40 \text{ kDa}}$  of the proximal tubule epithelium. A:  $GP_{70 \text{ kDa}/40 \text{ kDa}}$  image calculated using the autofluorescence signals captured by the detectors used to capture the 70-kDa FITC dextran and the 40-kDa tetramethylrhodamine dextran signals, respectively. B: distributions of the autofluorescence  $GP_{70 \text{ kDa}/40 \text{ kDa}}$  (yellowish green dashed line) and the  $\Delta GP_{70 \text{ kDa}/40 \text{ kDa}}$  of the proximal tubule epithelium (area 1 in Fig. 1, solid green line).

( $-0.659$ ) <  $\Delta GP_{40 \text{ kDa}/3 \text{ kDa}}$  ( $-0.502$ ). This suggests that the filtration rates of these dextrans had the following order (from fast to slow): 3-, 40-, and 70-kDa dextrans. It is striking that both the 40- and 70-kDa dextrans passed through the glomerular filtration barriers almost immediately after infusion of the dyes (Fig. 2). The hydrodynamic radius of the 70-kDa dextran is  $\sim 6.5$  nm (1), which is significantly larger than the 3.5-nm radius of albumin. The fact both the 40- and 70-kDa dextrans appeared so quickly in Bowman's space suggests that the glomerular wall was highly permeable to these dextrans. To our knowledge, this ultrafast glomerular leakage has not been reported previously in studies of glomerular permeability using MWF rats. The origin of this high glomerular capillary permeability to the 70-kDa FITC dextran can be attributed to the glomerular endothelium, the basement membrane, and the cellular and molecular machinery controlling the slit diaphragm (7) in addition to the shape and deformability of the dextran molecule (33). It was recently suggested that an alteration of a protein component of the slit diaphragm could significantly affect the permeability of the glomerular wall to

Table 5. 66 s after dextran infusion measured in healthy Sprague-Dawley rats

$\Delta GP$	Brush-Border Membrane	Proximal Tubular Lumen	Blood Vessel
$\Delta GP_{40 \text{ kDa anionic}/40 \text{ kDa neutral}}$ , $\pm$ FWHM	$0.254 \pm 0.182$	$-0.179 \pm 0.210$	$0.0074 \pm 0.183$

Data are from ROI indicated in Fig. 7.

albumin molecules (34). Because glomerular permeability is important in kidney studies, our aim was to develop an imaging technique that would allow us to follow concentration ratios of molecules with different sizes over time to facilitate these studies.

**Reabsorption of dextrans by the proximal tubules.** An interesting issue regarding glomerular permeability is its charge selectivity. The traditional view of the glomerular filter is that its molecular selectivity is based on size, shape, and charge. The combined effect is a filtration barrier that prevents large and negatively charged molecules from reaching Bowman's space (6, 8, 17, 21). It was recently proposed that polyanionic "plugs" exist in the endothelium of the glomerulus and that they electrostatically repel negatively charged macromolecules and prevent their filtration (24, 25). This concept was challenged by the experimental results using Ficoll and dextrans (12, 13, 27) that showed that the negative selectivity of glomerular filtration does not exist. We think that this controversy regarding glomerular charge selectivity is due in part to the lack of direct in vivo experimental methods that can separate and resolve glomerular filtration unambiguously from renal tubular reabsorption and enzymatic processing.

With regard to the results we reported in Figs. 1–3, we used the 70-kDa FITC-conjugated dextran, which was negatively charged (IP = 4.58), and the 40-kDa tetramethylrhodamine-conjugated dextran, which was neutral. The fact that both of these dextrans were present in Bowman's space was discussed above. As we have pointed out, the 70-kDa FITC dextran was preferentially reabsorbed by the brush-border membrane of the epithelial cells inside the proximal tubules (Fig. 3, C and C'), despite the fact that the  $\Delta GP_{70 \text{ kDa}/40 \text{ kDa}}$  value was relatively low in the Bowman's space, with an average of  $\Delta GP_{70 \text{ kDa}/40 \text{ kDa}} = -0.177$  (Table 2). In other words, proximal tubules reabsorb negatively charged dextrans more effectively than neutral dextrans. This effect of preferential reabsorption of the negatively charged 70-kDa FITC dextran by the proximal tubules was also evident in that the average  $\Delta GP_{70 \text{ kDa}/40 \text{ kDa}}$  value of the lumen was smaller than that of Bowman's space (Table 2 and Fig. 2, C and C'). At 4 s after dye infusion, the average  $\Delta GP_{70 \text{ kDa}/40 \text{ kDa}}$  was around  $-0.2$  inside the proximal tubule (negative  $\Delta GP$  indicates that the molecular ratio of 70-kDa to 40-kDa dextran was less than that of the dextran mixture being infused). At 36 min after dye infusion, the average  $\Delta GP_{70 \text{ kDa}/40 \text{ kDa}}$  inside distal tubules was less than  $-0.6$ , significantly smaller than the amount found in the proximal tubules. On the basis of these results, it is reasonable to conclude that the neutrally charged molecules, such as the 40-kDa tetramethylrhodamine dextran, are not reabsorbed as well as the negatively charged molecules. To further confirm this result, we performed  $\Delta GP$  imaging in Sprague-Dawley rats using two 40-kDa dextrans with different charges (Fig. 7). We found higher accumulations of the 40-kDa

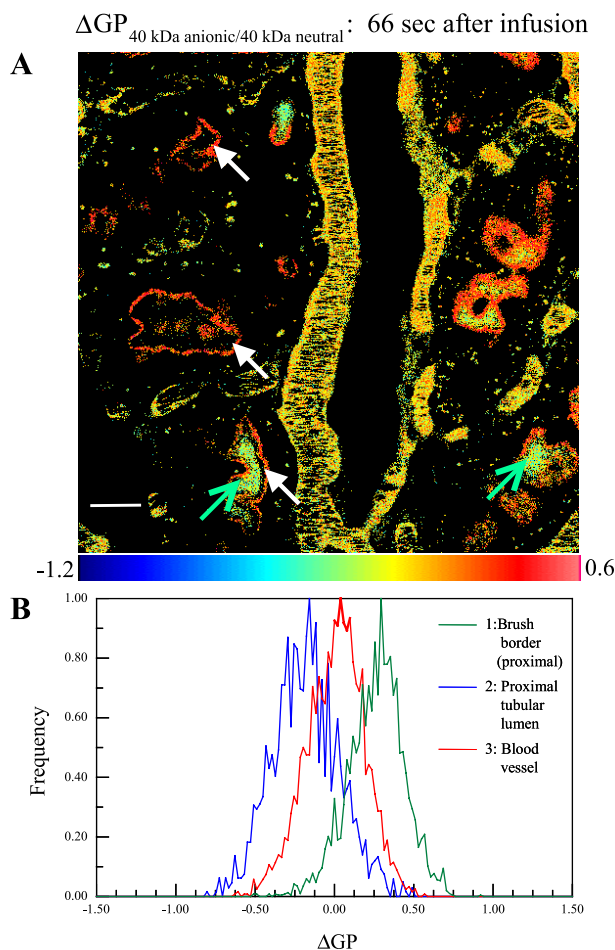


Fig. 7. Differential reabsorption of 40-kDa dextrans with different charges by the proximal tubule. A:  $\Delta GP_{40 \text{ kDa anionic}/40 \text{ kDa neutral}}$  image acquired from a Sprague-Dawley rat at 66 s after a mixture of 40-kDa FITC dextran (negatively charged) and 40-kDa tetramethylrhodamine dextran (neutral) was infused. B:  $\Delta GP_{40 \text{ kDa anionic}/40 \text{ kDa neutral}}$  distributions of the proximal brush-border membrane areas indicated by white arrows (green line), the proximal tubule lumens indicated by green arrows (blue line), and the blood plasma (red line). Scale bar, 20  $\mu\text{m}$ .

negatively charged dextran by the proximal brush-border membrane (Fig. 7A, areas indicated by white arrows), shown in red, with an average pixel value of  $\Delta GP_{40 \text{ kDa anionic}/40 \text{ kDa neutral}} = 0.254$  (Table 5). In contrast, there were more neutral 40-kDa dextran molecules in the proximal tubular lumen (Fig. 7A), shown in green, with an average of  $\Delta GP_{40 \text{ kDa anionic}/40 \text{ kDa neutral}} = -0.179$ . The fact that the  $\Delta GP_{40 \text{ kDa anionic}/40 \text{ kDa neutral}}$  value for the blood vessel was close to zero (Table 5) suggests that both the 40-kDa negatively charged and neutral dextrans were equally filtered. This result further confirms clearly that there was a preferential reabsorption of the negatively charged 40-kDa dextran by the proximal tubular cells compared with the neutral 40-kDa dextran. Note that the amount of the dextrans reabsorbed by the proximal tubule was minute compared with the amount moving through the renal tubular lumens. Therefore, one might not detect significant tubular reabsorption of dextrans by using a fractional clearance method (2, 3). In contrast, using GP microscopy, we directly evaluated tubular reabsorption with potentially single-molecule sensitivity. Molecular charges have previously been shown to play fundamental roles in proximal tubular uptake (4, 19). The understanding of charge-selective properties of renal tubules in reabsorbing charged molecules is important and may help to clarify issues regarding glomerular permeability (5, 20).

**Summary.** We have developed an intravital GP microscopic imaging technique that allows quantitative analysis of kidney functions in terms of glomerular filtration and tubular reabsorption. To demonstrate this microscopic technique, we imaged MWF rats with surface glomeruli. We observed fluorescence-tagged dextrans (both 40- and 70-kDa dextrans) with hydrodynamic radii larger than albumin present in the Bowman's space a few seconds after dye infusion. This ultrafast filtration process was associated with fast proximal tubular reabsorption of the dextran molecules. The differences in filtration and tubular reabsorption among the 3-, 40-, and 70-kDa dextrans were quantified, and the results suggest that tubular reabsorption is charge selective, with negatively charged dextrans being reabsorbed more effectively. Work is under way using the GP imaging technique to further understand the charge permselectivity of the glomerular filtration barrier and to quantify glomerular filtration rates.

#### ACKNOWLEDGMENTS

We thank Dr. Silvia B. Campos for performing animal surgeries, Xianming Chen for technical support, and the Indiana Center for Biological Imaging for the use of its microscopic imaging facility. We also thank Dr. Robert Bacallao for support and stimulating discussions and Dr. Pierre Dagher for critical reading of the manuscript and for providing valuable comments.

#### GRANTS

This work was supported by startup funds from an Indiana Genomics Initiative (INGEN) grant from the Eli Lilly and Company Foundation to Indiana University School of Medicine (to W. Yu) and a pilot study fund from an National Institutes of Health (NIH) O'Brien Center of Excellence grant (to W. Yu). Indiana Center for Biological Imaging is supported by funds from the INGEN grant and NIH O'Brien Center of Excellence Award P50 DK-61594 (to B. A. Molitoris).

#### REFERENCES

1. **Armstrong JK, Wenby RB, Meiselman HJ, and Fisher TC.** The hydrodynamic radii of macromolecules and their effect on red blood cell aggregation. *Biophys J* 87: 4259–4270, 2004.
2. **Bennett CM, Glasscock RJ, Chang RL, Deen WM, Robertson CR, Brenner BM, Troy JL, Ueki IR, and Rasmussen B.** Permselectivity of the glomerular capillary wall: studies of experimental glomerulonephritis in the rat using dextran sulfate. *J Clin Invest* 57: 1287–1294, 1976.
3. **Chang RL, Deen WM, Robertson CR, and Brenner BM.** Permselectivity of the glomerular capillary wall. III. Restricted transport of poly-anions. *Kidney Int* 8: 212–218, 1975.
4. **Christensen EI, Rennke HG, and Carone FA.** Renal tubular uptake of protein: effect of molecular charge. *Am J Physiol Renal Fluid Electrolyte Physiol* 244: F436–F441, 1983.
5. **Comper WD.** Charge selectivity is a concept that has yet to be demonstrated (Letter). *Am J Physiol Renal Physiol* 281: F992–F993, 2001.
6. **D'Amico G and Bazzi C.** Pathophysiology of proteinuria. *Kidney Int* 63: 809–825, 2003.
7. **Deen WM.** What determines glomerular capillary permeability? *J Clin Invest* 114: 1412–1414, 2004.
8. **Deen WM, Lazzara MJ, and Myers BD.** Structural determinants of glomerular permeability. *Am J Physiol Renal Physiol* 281: F579–F596, 2001.
9. **Denk W, Strickler JH, and Webb WW.** 2-Photon laser scanning fluorescence microscopy. *Science* 248: 73–76, 1990.
10. **Dunn KW, Sandoval RM, Kelly KJ, Dagher PC, Tanner GA, Atkinson SJ, Bacallao RL, and Molitoris BA.** Functional studies of the kidney of living animals using multicolor two-photon microscopy. *Am J Physiol Cell Physiol* 283: C905–C916, 2002.
11. **Dunn KW, Sandoval RM, and Molitoris BA.** Intravital imaging of the kidney using multiparameter multiphoton microscopy. *Nephron Exp Nephrol* 94: e7–e11, 2003.
12. **Greive KA, Nikolic-Paterson DJ, Guimarães MAM, Nikolovski J, Pratt LM, Mu W, Atkins RC, and Comper WD.** Glomerular permselectivity factors are not responsible for the increase in fractional clearance of albumin in rat glomerulonephritis. *Am J Pathol* 159: 1159–1170, 2001.
13. **Guimarães MAM, Nikolovski J, Pratt LM, Greive K, and Comper WD.** Anomalous fractional clearance of negatively charged Ficoll relative to uncharged Ficoll. *Am J Physiol Renal Physiol* 285: F1118–F1124, 2003.
14. **Li B, Yao J, Kawamura K, Oyanagi-Tanaka Y, Hoshiyama M, Morioka T, Gejyo F, Uchiyama M, and Oite T.** Real-time observation of glomerular hemodynamic changes in diabetic rats: effects of insulin and ARB. *Kidney Int* 66: 1939–1948, 2004.
15. **Meyer TW and Rennke HG.** Progressive glomerular injury after limited renal infarction in the rat. *Am J Physiol Renal Fluid Electrolyte Physiol* 254: F856–F862, 1988.
16. **Molitoris BA, Sandoval R, and Sutton TA.** Endothelial injury and dysfunction in ischemic acute renal failure. *Crit Care Med* 30, Suppl 5: S235–S240, 2002.
17. **Ohlson M, Sörensson J, and Haraldsson B.** Glomerular size and charge selectivity in the rat as revealed by FITC-Ficoll and albumin. *Am J Physiol Renal Physiol* 279: F84–F91, 2000.
18. **Oliver JD III, Anderson S, Troy JL, Brenner BM, and Deen WH.** Determination of glomerular size-selectivity in the normal rat with Ficoll. *J Am Soc Nephrol* 3: 214–228, 1992.
19. **Osicka TM and Comper WD.** Glomerular charge selectivity for anionic and neutral horseradish peroxidase. *Kidney Int* 47: 1630–1637, 1995.
20. **Osicka TM, Strong KJ, Nikolic-Paterson DJ, Atkins RC, and Comper WD.** Albumin and glomerular permselectivity (Letter). *Nephrol Dial Transplant* 19: 511–512, 2004.
21. **Pavenstädt H, Kriz W, and Kretzler M.** Cell biology of the glomerular podocyte. *Physiol Rev* 83: 253–307, 2003.
22. **Peti-Peterdi J, Fintha A, Fuson AL, Tousson A, and Chow RH.** Real-time imaging of renin release in vitro. *Am J Physiol Renal Physiol* 287: F329–F335, 2004.
23. **Peti-Peterdi J, Morishima S, Bell PD, and Okada Y.** Two-photon excitation fluorescence imaging of the living juxtaglomerular apparatus. *Am J Physiol Renal Physiol* 283: F197–F201, 2002.
24. **Rippe B.** What is the role of albumin in proteinuric glomerulopathies? *Nephrol Dial Transplant* 19: 1–5, 2004.
25. **Rostgaard J and Qvortrup K.** Sieve plugs in fenestrae of glomerular capillaries: site of the filtration barrier? *Cells Tissues Organs* 170: 132–138, 2002.
26. **Sandoval RM, Kennedy MD, Low PS, and Molitoris BA.** Uptake and trafficking of fluorescent conjugates of folic acid in intact kidney deter-

- mined using intravital two-photon microscopy. *Am J Physiol Cell Physiol* 287: C517–C526, 2004.
27. **Schaeffer RC Jr, Gratrix ML, Mucha DR and Carbajal JM.** The rat glomerular filtration barrier does not show negative charge selectivity. *Microcirculation* 9: 329–342, 2002.
  28. **Schulz A, Litfin A, Kossmehl P, and Kreutz R.** Genetic dissection of increased urinary albumin excretion in the Munich Wistar Frömter rat. *J Am Soc Nephrol* 13: 2706–2714, 2002.
  29. **Schulz A, Standke D, Kovacevic L, Mostler M, Kossmehl P, Stoll M, and Kreutz R.** A major gene locus links early onset albuminuria with renal interstitial fibrosis in the MWF rat with polygenetic albuminuria. *J Am Soc Nephrol* 14: 3081–3089, 2003.
  30. **Sutton TA, Fisher CJ, and Molitoris BA.** Microvascular endothelial injury and dysfunction during ischemic acute renal failure. *Kidney Int* 62: 1539–1549, 2002.
  31. **Sutton TA, Mang HE, Campos SB, Sandoval RM, Yoder MC, and Molitoris BA.** Injury of the renal microvascular endothelium alters barrier function after ischemia. *Am J Physiol Renal Physiol* 285: F191–F198, 2003.
  32. **Tanner GA, Sandoval RM, and Dunn KW.** Two-photon in vivo microscopy of sulfonefluorescein secretion in normal and cystic rat kidneys. *Am J Physiol Renal Physiol* 286: F152–F160, 2004.
  33. **Venturoli D and Rippe B.** Ficoll and dextran vs. globular proteins as probes for testing glomerular permselectivity: effects of molecular size, shape, charge, and deformability. *Am J Physiol Renal Physiol* 288: F605–F613, 2005.
  34. **Wartiovaara J, Öfverstedt LG, Khoshnoodi J, Zhang J, Mäkelä E, Sandin S, Ruotsalainen V, Cheng RH, Jalanko H, Skoglund U, and Tryggvason K.** Nephrin strands contribute to a porous slit diaphragm scaffold as revealed by electron tomography. *J Clin Invest* 114: 1475–1483, 2004.
  35. **Yu W, So PT, French T, and Gratton E.** Fluorescence generalized polarization of cell membranes: a two-photon scanning microscopy approach. *Biophys J* 70: 626–636, 1996.

